

Structural and Functional Basis for ADP-Ribose and Poly(ADP-Ribose) Binding by Viral Macro Domains

Marie-Pierre Egloff,^{1†} Hélène Malet,^{1†} Ákos Putics,² Maarit Heinonen,⁴ Hélène Dutartre,¹
Antoine Frangeul,¹ Arnaud Gruez,¹ Valérie Campanacci,¹ Christian Cambillau,¹
John Ziebuhr,^{2,3} Tero Ahola,⁴ and Bruno Canard^{1*}

Centre National de la Recherche Scientifique and Universités d'Aix-Marseille I et II, UMR 6098, Architecture et Fonction des Macromolécules Biologiques, Ecole Supérieure d'Ingénieurs de Luminy–Case 925, 163 Ave. de Luminy, 13288 Marseille Cedex 9, France¹; Institute of Virology and Immunology, University of Würzburg, Versbacher Strasse 7, 97078 Würzburg, Germany²; Centre for Cancer Research and Cell Biology, School of Biomedical Sciences, The Queen's University of Belfast, 97 Lisburn Rd., Belfast BT9 7BL, United Kingdom³; and Program in Cellular Biotechnology, Institute of Biotechnology, University of Helsinki, P.O. Box 56, Viikinkaari 9, 00014 Helsinki, Finland⁴

Received 23 May 2006/Accepted 8 June 2006

Macro domains constitute a protein module family found associated with specific histones and proteins involved in chromatin metabolism. In addition, a small number of animal RNA viruses, such as corona- and toroviruses, alphaviruses, and hepatitis E virus, encode macro domains for which, however, structural and functional information is extremely limited. Here, we characterized the macro domains from hepatitis E virus, Semliki Forest virus, and severe acute respiratory syndrome coronavirus (SARS-CoV). The crystal structure of the SARS-CoV macro domain was determined at 1.8-Å resolution in complex with ADP-ribose. Information derived from structural, mutational, and sequence analyses suggests a close phylogenetic and, most probably, functional relationship between viral and cellular macro domain homologs. The data revealed that viral macro domains have relatively poor ADP-ribose 1''-phosphohydrolase activities (which were previously proposed to be their biologically relevant function) but bind efficiently free and poly(ADP-ribose) polymerase 1-bound poly(ADP-ribose) *in vitro*. Collectively, these results suggest to further evaluate the role of viral macro domains in host response to viral infection.

Positive-strand RNA viruses employ an RNA-dependent RNA polymerase to replicate their single-stranded genomic RNA. In most cases, this polymerase is associated with other (viral or cellular) proteins, such as RNA helicases, RNA capping enzymes, and proteins of yet-unknown function. Besides a direct role in viral RNA synthesis, it has become increasingly clear that some of the polymerase-associated proteins have evolved to counteract or modify host defense pathways.

Coronaviridae (genera *Coronavirus* and *Torovirus*) have the largest single-stranded RNA genomes (27 to 31.5 kb) identified to date (12, 38). Thus, for example, severe acute respiratory syndrome coronavirus (SARS-CoV) is predicted to encode as many as 28 proteins, for most of which the functions are unknown. The coronavirus replicative proteins, commonly known as nonstructural proteins (nsp) 1 to 16, are expressed from an unusually large replicase gene of more than 20 kilobases that consists of two large open reading frames (ORF1a and ORF1b), with the expression of the latter involving a ribosomal frameshift that occurs just upstream of the ORF1a translation stop codon (4). The translation products expressed from ORF1a and ORF1b are called replicase polyproteins, pp1a (>4,000 amino acids [aa]) and pp1ab (>7,000 aa). The two polyproteins are cleaved by viral proteinases, and the vast

majority of the proteolytic processing products assemble into a membrane-associated viral replication/transcription complex. The coronavirus nsp3 is the largest of these processing products and has been predicted to harbor several conserved domains and enzymatic activities (39, 42, 43), including a macro domain that is often in the context of viruses referred to as X domain (13).

Macro domains are conserved in a wide variety of bacteria, archaea, and eukaryotes. Their name refers to the non-histone domain of the histone macroH2A (29). In animal cells, macro domains are in some cases found physically associated with proteins involved in ADP-ribosylation or poly(ADP-ribose) polymerization, as well as in ATP-dependent chromatin remodeling (1). This linkage, together with their ubiquitous distribution, suggest that macro domains may be involved in diverse pathways, including ADP-ribose metabolism and post-translational protein modification. Apart from all family members of the *Coronaviridae*, very few other viruses possess macro domains. These include rubella virus and alphaviruses (family *Togaviridae*), as well as hepatitis E virus (HEV) (39). The role(s) of macro domains in the replication of these positive-strand RNA viruses or in interactions with their hosts has remained elusive. The presence of macro domains in just a small set of virus families is puzzling and, thus far, could not be related to any specific feature shared exclusively by macro the domain-encoding *Coronaviridae*, *Togaviridae*, and HEV. Furthermore, recent coronavirus reverse genetics data argued against an essential role of the macro domain in viral replication in tissue culture (30). Based on this observation and the

* Corresponding author. Mailing address: Architecture et Fonction des Macromolécules Biologiques, UMR 6098 CNRS et Université Aix-Marseille I et II, ESIL, Campus de Luminy, 13288 Marseille Cedex 09, France. Phone: 33 4 91 82 86 44. Fax: 33 4 91 82 86 46. E-mail: Bruno.Canard@afmb.univ-mrs.fr.

† M.-P.E. and H.M. contributed equally to this study.

nonessential function of a cellular macro domain from yeast, it has been speculated that macro domains might have regulatory rather than essential functions (13, 30, 37, 39).

The first direct biochemical information concerning macro domains indicated that they might be involved in the downstream processing of ADP-ribose 1"-phosphate, a side product of cellular pre-tRNA splicing (22, 30, 39), thus controlling the metabolism of ADP-ribose 1"-phosphate or other ADP-ribose derivatives with known regulatory functions in the cell. ADP-ribose 1"-phosphatase (Appr-1"-pase) activities have been demonstrated for a yeast macro domain, the AF1521 protein of *Archaeoglobus fulgidus*, as well as for three coronaviruses, namely, human coronavirus 229E (HCoV-229E), transmissible gastroenteritis virus, and SARS-CoV (22, 30, 31, 33, 39). In all of these cases, the enzyme turned out to be highly specific for ADP-ribose 1"-phosphate but, for an enzyme supposed to be involved in metabolic regulation, was poorly active as judged by its turnover constant, k_{cat} (1.7 to 20 min^{-1}). Furthermore, the facts that (i) inactivation of the macro domain's enzymatic activity in HCoV-229E does not apparently affect viral RNA synthesis in vitro and (ii) no complete RNA processing pathway can be inferred from the ADP-ribose 1"-phosphatase (and the much less conserved ADP-ribose 1",2" cyclic phosphodiesterase) activities would argue against a direct role in viral RNA synthesis and suggest alternative functions for these domains. Other possible functions of macro domains could relate to virus interactions with the host, for example, by counteracting cellular responses, such as apoptosis, elicited by the products or intermediates of viral genome and subgenome RNA synthesis or by specific viral or virus-induced proteins (reviewed in reference 15). This idea is supported by the close functional association of macro domains with poly(ADP-ribose) polymerase 1 (PARP-1), which is known to be involved in the regulation of apoptosis in eukaryotic cells (2). In support of possible roles of viral macro domains in cellular signaling, including ADP-ribose-generating or -consuming pathways, an archaeal macro domain was recently demonstrated to act as a high-affinity ADP-ribose and poly(ADP-ribose)-binding module (17).

During the course of the present study, the crystal structure of the unliganded SARS-CoV macro domain was determined independently (33). The purified protein was shown to bind ADP-ribose and have ADP-ribose 1"-phosphatase activity. However, the determinants for enzymatic activity and ADP-ribose binding were not studied, and the relevance of this activity in either virus-cell interactions or metabolic pathway regulation is still obscure.

We have determined here the crystal structure of the SARS-CoV macro subdomain of the nsp3 gene product at $1.8\text{-}\text{\AA}$ resolution in complex with ADP-ribose and investigated representative proteins from three virus families encoding macro domains. Both our structural analysis of the binary complex and functional data lead us to reconsider the previously proposed biological role of viral macro domains as ADP-ribose 1"-phosphatases. Here we demonstrate that viral macro domains are efficient poly(ADP-ribose) binding modules, suggesting a link to poly(ADP-ribose) signaling pathways.

MATERIALS AND METHODS

Preparation of recombinant macro domain proteins. The recombinant SARS-CoV macro domain (residues 182 to 355 of SARS-CoV nsp3) was expressed in

TABLE 1. Diffraction, structure determination, and refinement statistics

Parameter	Data
Diffraction data	
Space group	P2 ₁
Cell dimensions	a = 37.45 \AA , b = 55.50 \AA , c = 108.93 \AA , β = 91.39°
Wavelength (\AA)	0.9792
Spacing limit (\AA)	1.8
Unique reflections	41,654
R_{merge} (%) ^a	10.8 (38.6)
I/σ	17.7 (7.1)
Completeness (%)	99.9 (99.9)
Anomalous completeness (%)	99.9 (99.9)
Multiplicity	10.4 (8.9)
Phasing and refinement	
Bragg spacings (\AA)	28-1.8
Figure of merit after RESOLVE	0.75
No. of protein atoms	3,851
No. of solvent atoms	482
No. of hetero-atoms (ADP-ribose)	35
$R_{\text{work}}/R_{\text{free}}^c$ (%)	15.1/19.5
Avg B factor (\AA^2)	10.613
Rms deviation of bond lengths (\AA)	0.018
Rms deviation of bond angles (°)	1.85
Ramachandran plot ^d	91.1/8.9

^a $R_{\text{merge}} = \sum |I - \langle I \rangle| / \sum I$, where I is the observed intensity and $\langle I \rangle$ is the average intensity. Values in parentheses refer to the highest-resolution shell (1.9 to 1.8).

^b $R = \sum ||F_o| - |F_c|| / \sum |F_o|$.

^c R_{free} is calculated as R , but on 5% of all reflections that are never used in crystallographic refinement.

^d The percentage of residues located in the most favorable/additionally allowed regions of the Ramachandran plot is given.

Escherichia coli after cloning of the corresponding gene region (isolate Frankfurt 1, DDBJ/EMBL/GenBank accession number AY291315) into pDEST14 plasmid (Invitrogen). A detailed report on cloning, expression, and purification is reported elsewhere (21). Mutant forms of this protein were produced by codon mutagenesis of plasmid pDEST14 (Invitrogen) using PCR-based methods as described previously (30). Recombinant HEV macro domain (residues 775 to 960 of the Burmese strain) was expressed as N terminally histidine-tagged protein in *E. coli*. The protein was purified by Ni affinity chromatography and stored in 25 mM HEPES (pH 8.0), 250 mM NaCl, 1 mM dithiothreitol, and 20% glycerol at -70°C . A recombinant Semliki Forest virus (SFV) NSP3 domain (residues 1336 to 1669 of the polyprotein; DDBJ/EMBL/GenBank accession number X04129) was expressed in *E. coli* as an N terminally hexahistidine-tagged protein. It was purified by Ni and size exclusion chromatographies and stored in 10 mM CHES-300 mM NaCl (pH 9.0).

Computer-aided comparative sequence analyses. Amino acid sequences were retrieved from the Swissprot database. Sequence alignments were produced by using the program MUSCLE (9), manually edited using SEAVIEW (10), and processed for presentation using ESPRIPT (14). Secondary structure predictions were performed by using the JPRED server (7).

Structure determination of SARS-CoV macro domain. Crystallization of the SARS-CoV macro domain has been reported elsewhere (21). The structure was resolved by using an SAD data set collected on a Se-Met substituted crystal that had been soaked for 2 h in 2 mM ADP-ribose prior to flash-freezing and data collection. A complete data set (99.9% of the anomalous data have been collected, see Table 1) was collected up to $1.8\text{-}\text{\AA}$ resolution. The data were processed with MOSFLM and reduced and scaled by using the SCALA program from the CCP4 suite (6). Crystals belong to space group P2₁ with the following unit cell dimensions: a = 37.450 \AA , b = 55.550 \AA , c = 108.920 \AA , and β = 91.39°. The asymmetric unit contains three monomers (designated molecules A, B, and C, respectively), giving a VM value of $2.0 \text{ \AA}^3 \text{ Da}^{-1}$ and 38.9% solvent. The data on the SeMet-substituted crystal were collected at the absorption peak (λ = 0.9792 \AA) (Table 1) and phased by using the SAD method. Eight of the nine SeMet positions were determined by the program SOLVE (41) and used for the

initial phase determination. Density modification performed with the program RESOLVE (40) produced a map of excellent quality, in which the ARP/wARP (5) program could build residues 2 to 171 of one of the monomers (comprising a total of 173 aa). Five percent of the observations were set apart for cross-validation and were used to monitor refinement strategies such as temperature factor and geometric restraint values. Manual corrections of the model using the program TURBO-FRODO (32) alternate with cycles of least-squares refinement using the maximum-likelihood program REFMAC (25). Water molecules were added automatically using the ARP/wARP program and then inspected manually. The ADP-ribose molecule dictionary was extracted from the "monomer library sketcher" in the CCP4 suite. The model was validated by using PROCHECK (20). The root-mean-squared deviation between ideal and real values of bond length and angle are 0.018 Å and 1.85°, respectively (Table 1), and 99.9% of the residues were located in the allowed regions of the Ramachandran plot (Table 1), attesting to the excellent quality of the model. The coordinates have been deposited in the Protein Data Bank under accession number 2FAV.

ADP-ribose binding. Isothermal titration binding assays were performed at 30°C using a VP-ITC instrument (Microcal). Reactions were carried out in 10 mM MOPS (pH 7.0)–150 mM NaCl, using 30 or 45 µM SARS-CoV or HEV macro domain, and successive injections of 350 µM ADPR or 500 µM ADP, respectively. The data was analyzed by using Origin software (OriginLab).

Assay for Appr-1"-pase activity. Appr-1"-pase activity of HEV macro domain was detected by using thin-layer chromatography (TLC) assays. First, Appr-1"-phosphate was produced by incubating 7 mM ADP-ribose 1"-2"-cyclic phosphate (Appr>p) with cyclic phosphodiesterase (15 ng/ml) for 3 h at 28°C. Cyclic phosphodiesterase was then inactivated at 94°C for 2 min. Then, 1 µl of the first reaction was mixed with 1 µl of 50 µM HEV macro domain protein in 20 mM HEPES (pH 7.4) and 1 µl of 60 mM MES (morpholineethanesulfonic acid; pH 5.0). The reaction mixture was incubated at 28°C for 2 h. A total of 2 µl of the reaction mixture was then spotted onto PEI-F cellulose TLC, and the plate was developed at room temperature in 0.15 M NaCl–0.15 M sodium formate (pH 3.0). The spots were detected from the fluorescent background under a UV lamp at 254-nm wavelength. A very close protocol was used to test the Appr-1"-pase activity of SARS-CoV macro domain (as described in reference 30). Equivalent concentrations of bovine serum albumin (BSA) were used as a negative controls.

Poly(ADP-ribose) synthesis and binding assay. Poly(ADP-ribose) (PAR), a branched homopolymer of ADP-ribose units linked mainly by glycosidic 1"-2' bonds, was synthesized by auto-ADP-ribosylation of PARP-1 in 100 µl of 25 mM Tris (pH 8), 10 mM MgCl₂, 100 mM NaCl, 0.5 mM dithiothreitol, and 6 mg of activated calf DNA/ml using 0.8 U of hPARP (Sigma), 150 mM NAD, and 0.5 mCi of ³²P-labeled NAD⁺ (Amersham-Pharmacia). In control reactions, hPARP-1 was omitted. After 1 h at 25°C under agitation, the reaction was stopped by dilution with either 140 µl of 10 mM morpholinepropanesulfonic acid (MOPS)–150 mM NaCl (PAR-binding buffer) or 2.5 µl of 10 mM MOPS–150 mM NaCl–0.05% Tween 20 (Dot-Blot buffer). Alternatively, the reaction was stopped by DNase treatment, and PAR was purified after degradation of hPARP-1 using proteinase K.

For PAR-binding assays on beads, increasing concentrations of SARS-CoV macro domain were incubated in 100 µl of PAR-binding buffer with 40 µl of diluted radiolabeled PAR for 1 h at 25°C under agitation. His-tagged proteins were then precipitated by the addition of nitrilotriacetic acid-beads equilibrated in PAR-binding buffer. Beads were washed three times in PAR-binding buffer and resuspended in 100 µl of formaldehyde loading buffer. Samples were boiled 3 min, and 10 µl was loaded on 20% polyacrylamide-urea gel. Products were separated by electrophoresis in Tris-borate-EDTA and visualized with a PhosphorImager.

For the blotting assay, the macro domains of SARS-CoV (28, 14, 7, 3.5, 1.75, 0.8, or 0.4 nmol), SFV (13, 6.5, 3.2, 1.6, 0.8, 0.4, 0.2, or 0.1 nmol), or HEV (1.5, 0.2, or 0.02 nmol) were blotted on nitrocellulose membrane using a Minifold II dot blot or a slot blot apparatus (Schleicher & Schuell). Membranes were blocked for 1 h in Dot-Blot buffer containing 5% dry milk powder and subsequently incubated for 1 h with the PAR preparation or the purified PAR preparation diluted in the Dot-Blot buffer. After extensive washes, the membrane-bound fraction of PAR was measured by PhosphorImager analysis.

Molecular modeling. Based on the refined coordinates of the ADP-ribose molecule found in the crystal structure, a di-ADP-ribose molecule was manually constructed by using the program TURBO-FRODO (32). We used the PRODRG (35) server to compute hydrogen atoms and atomic charges and to minimize the di-ADP-ribose molecule. The AutodockTools package (24) was used to generate the docking input files and analyze the docking results. Nonpolar hydrogen atoms and water molecules were removed from the input coordinate file, and the Kollmann charges were loaded on the protein atoms. The region of interest used by Autodock was defined in such a way to include a large portion around the

putative binding site. In particular, a grid of 90 points in x, y, and z directions with a spacing of 0.375 Å was built centered on the center of mass of the ADP-ribose binding site. The docking procedure was first validated by modeling of an ADP-ribose molecule in the apo-protein and checking that the result is superimposable with the actual ADP-ribose molecule as refined against the crystallographic data collected on the ADP-ribose–protein complex. For di-ADP-ribose modeling, the first module of ADP-ribose as revealed by the crystal structure was fixed, whereas all of the other bonds were treated as active torsional bonds. One hundred docked structures, i.e., 100 runs, were generated by using genetic algorithm searches. A default protocol was applied, with an initial population of 50 randomly placed individuals, a maximum number of 250,000 energy evaluations, and a maximum number of 27,000 generations. A mutation rate of 0.02 and a crossover rate of 0.8 were used. A cluster analysis was performed by using a root-mean-square tolerance of 1.0 Å.

RESULTS

Overall structure of the SARS-CoV macro domain. The protein is monomeric and globular, with approximate dimensions 40 Å × 40 Å × 35 Å. The asymmetric unit is made of three monomers that are roughly aligned (Fig. 1A). Each monomer consists of a central seven-stranded twisted mixed β-sheet (Fig. 1B). The order of the β-strands within the β-sheet is β1, β2, β7, β6, β3, β5 and β4. They are all parallel except for strands β1 and β7. This central β-sheet is sandwiched by two α-helices on one face and three on the other face. A last α-helix forms the C terminus of the protein and is located on the edge of the central β-sheet (Fig. 1B).

When searching the DALI database (16) with the conserved core of the SARS-CoV macro domain as a model (aa 15 to 26, 33 to 80, 87 to 99, and 106 to 148), the significant results in terms of structural similarity and functional relevance are macro domain structures from *E. coli* (unpublished, PDB code 1SPV), archaeal macro domain AF1521 (Z-score = 12.6) (2), and *H. sapiens* macroh2a1.1 and macroh2a1.2 (respective Z-scores = 11.9 and 11.7) (19). This reflects the fact that the central core of macro domains is structurally well conserved. The root-mean-squared deviation between the central β-sheet of the SARS-CoV macro domain and the macro domains of yeast, *Archaeoglobus fulgidus*, and *E. coli*, respectively, are 2.20 Å (on 130 amino acids), 2.09 Å (on 149 amino acids), and 1.97 Å (on 143 amino acids) (calculated using the server msdfold <http://www.ebi.ac.uk/msd-srv/ssm/cgi-bin/ssmserver>).

However, variability between all of these structures arises from (i) the loops connecting the core secondary structure elements, which display great diversity in sequence, length, and conformation; (ii) the N and C termini, and more particularly the relative orientation of the last α-helix (residues 159 to 173) compared to the central β-sheet; and (iii) some differences in the connectivity between the secondary structure elements as exemplified thus far by the yeast YMX7 crystal structure (18). The latter is the only structure of macro domains presenting an extra domain in addition to the α/β/α central core, which may be related to this connectivity change.

Structural and biochemical basis for ADP-ribose binding. It has been recently demonstrated that HCoV-229E, SARS-CoV, and transmissible gastroenteritis virus macro domains could act as phosphatases converting ADP-ribose 1"-monophosphate (Appr-1"-p) to ADP-ribose (Appr) (31). In order to elucidate the structural basis for this activity, we resolved the crystal structure of the SARS-CoV macro domain on a Se-Met crystal that had been soaked in 2 mM ADP-ribose

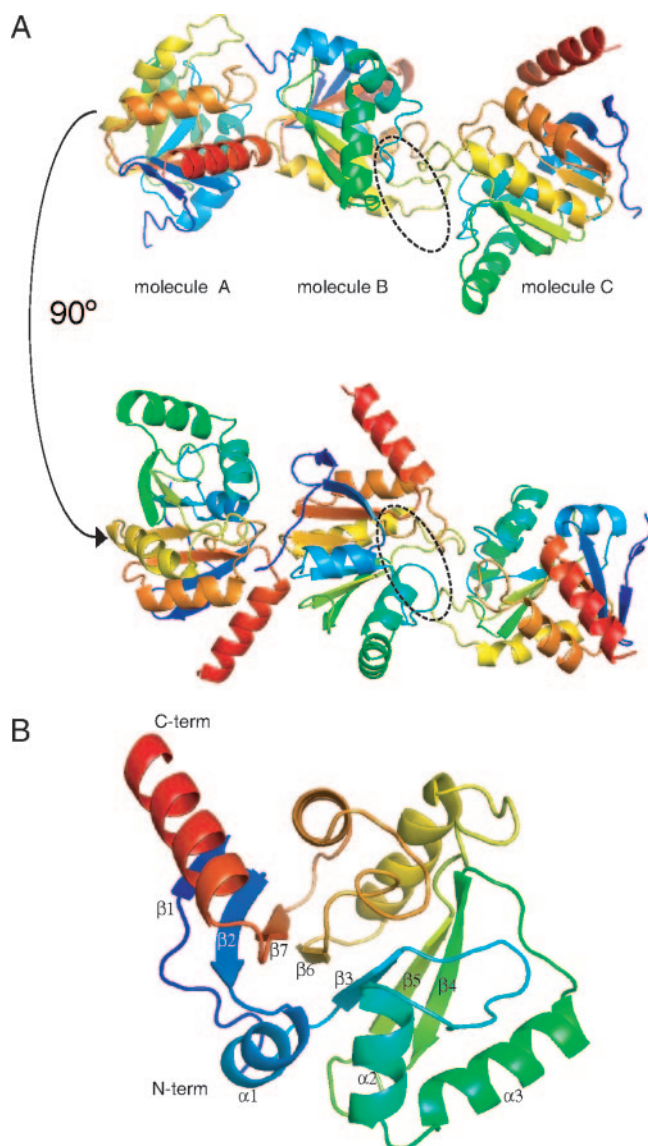


FIG. 1. Ribbon representation of the SARS-CoV macro domain. (A) Two views rotated by 90° display the arrangement of the three molecules present in the asymmetric unit, each of them colored in a purple-to-red gradient (from N terminus to C terminus). In one molecule of the asymmetric unit only (molecule B), the ADP-ribose binding site is accessible to solvent and is surrounded by dotted lines. (B) Secondary structure elements are explicitly labeled.

for 2 h. Amino acids 2 to 173 have been built and refined (Table 1), and only one residue at both termini of the protein is missing. After the first cycle of refinement, a strong bent density (continuous at 3 σ cutoff) (Fig. 2A), located near the surface of molecule B (central molecule as shown in Fig. 1A), could unambiguously be identified as an ADP-ribose molecule. This molecule is tightly bound in an uncharged crevice located at the C-terminal end of strands β_4 and β_5 in the loop regions between β_5 - α_2 and β_4 - α_5 . Analysis of the crystal packing revealed that the ADP-ribose binding sites of molecules A and C (Fig. 1A) were buried,

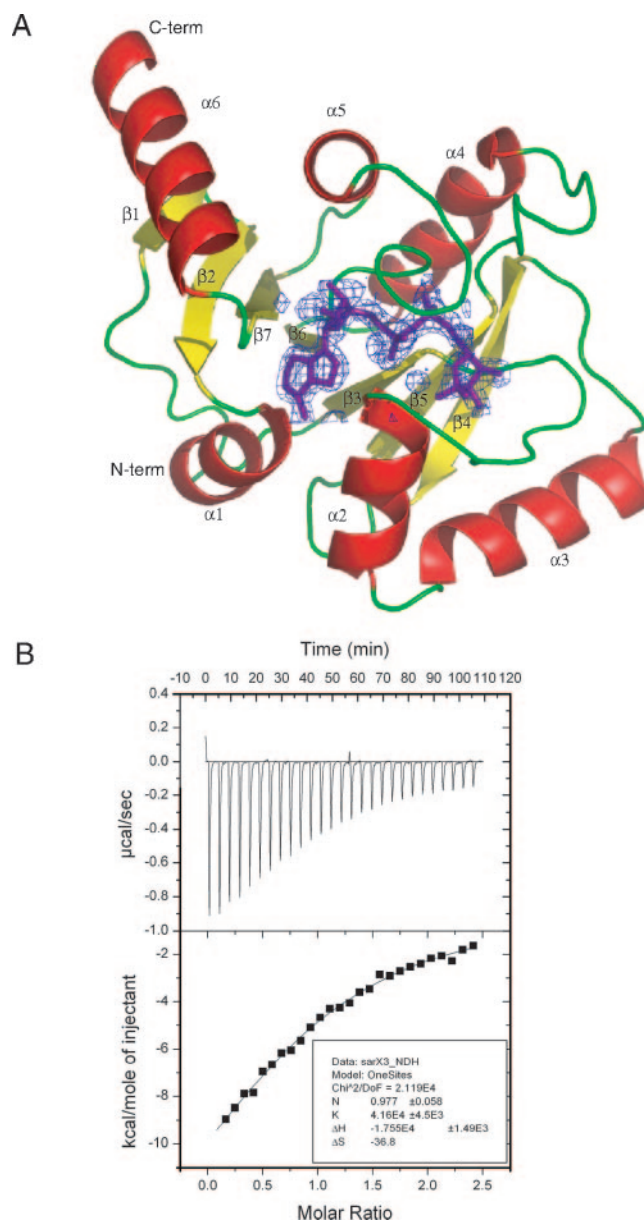


FIG. 2. ADP-ribose binding. (A) Representation of the σ_A -weighted $F_o - F_c$ Fourier map, contoured at 3 σ , as identified in the B molecule of the SARS-CoV macro domain during the first round of refinement. The final model of the ADP-ribose molecule is displayed in purple sticks in the purple electron density. The protein is represented in ribbons and colored according to secondary structure (α -helices in red, β -strands in yellow, and connecting loops in green). (B) Isothermal titration calorimetry profile for the binding of ADP-ribose to SARS-CoV macro domain.

thus clarifying why ADP-ribose could diffuse into molecule B exclusively.

The ADP-ribose molecule lies in a slightly bent conformation, partly buried in a mainly hydrophobic cleft located at the C-terminal side of the central β -sheet (Fig. 2A). The adenosine moiety lies in a hydrophobic pocket lined by residues coming from the C-terminal part of strands β_6 and β_7 , the loop connecting strand β_2 to helix α_1 and the N-terminal part of helix

$\alpha 2$. The adenine moiety is hydrogen bonded via its N6 nitrogen to the Asp-23 side chain and via its N1 nitrogen to the main chain HN of Ile-24. No steric hindrance is revealed when a guanine is modeled instead of an adenine. However, specificity for the adenosine moiety binding has been demonstrated in the case of the *A. fulgidus* macro domain AF1521 (17). This specificity is very likely provided by a strictly conserved aspartic acid residue located at the C terminus of the first strand, namely, Asp-23 in the SARS-CoV macro domain, since (i) an oxygen of this aspartic acid carboxyl group is hydrogen bonded to the NH2 atom at position 6 of the adenosine moiety; (ii) this hydrogen bond with the O atom at position 6 of a guanosine would require the deprotonation of Asp-23 carboxyl group, which cannot be performed by any surrounding residue; and (iii) mutation of this aspartic acid to alanine was shown to greatly reduce ADP-ribose and ADP binding in *A. fulgidus* (17). The distal ribose of ADP-ribose fits snugly into a narrow pocket made of three loops: loop 1 (residues 129 to 133), connecting strand $\beta 6$ and helix $\alpha 5$; loop 2, which consists of three conserved glycine residues (Gly-47 to Gly-49) and connects strand $\beta 3$ to helix $\alpha 2$; and loop 3 (residues 101 to 103), connecting strand $\beta 5$ to helix $\alpha 4$. The two phosphate groups are H bonded to the main chain NH groups of residues of loop 1, as well as the main chain NH group of the valine residue (Val-50) located at the end of loop 2 (see Fig. 5 below). Comparison of the ADP-ribose binding site as determined in the present study with that identified in yeast and *A. fulgidus* macro domains reveals that amino acids implicated in the interaction with ADP-ribose belong to motifs that are evolutionarily well conserved.

The binding of ADP-ribose to the SARS-CoV macro domain was confirmed by using isothermal titration calorimetry. This technique is often used in thermodynamic analyses of macromolecular interactions. It provides the basis for the determination of dissociation constants through the measurement of either absorbed or released heat upon binding of the two partners, using no chemical tagging nor immobilization of the interacting components. Using such a technique, we demonstrated that ADP-ribose bound to the SARS-CoV macro domain with an equilibrium dissociation constant (K_D) value of $\sim 24 \mu\text{M}$ (Fig. 2B). No detectable binding was found using ADP. When the same experiment was performed with the HEV macro domain, binding of ADP-ribose was clearly detected, but the K_D could not be reliably determined at the protein concentrations used ($K_D > 50 \mu\text{M}$) (not shown). The binding affinity of viral proteins is markedly lower than that of AF1521 ($K_D = 126 \text{ nM}$) (17) and MacroH2A1.1 ($2.7 \mu\text{M}$) (19).

Comparison of the ligand-free molecules A and C to the ADP-ribose complexed molecule B revealed that some conformational changes occurred upon ADP-ribose binding (Fig. 3). The loop comprising residues 98 to 107 undergoes a movement (with a maximal amplitude of 2.9 \AA), which results in a modest widening of the crevice in which the ribose moiety is located. Moreover, the two loops sandwiching ADP-ribose, namely, loop 2 (His-46, Gly-47, Gly-48, and Gly-49) and loop 3 (Ile-132 Phe-133), also undergo small changes upon ADP-ribose binding. Further refinement revealed that both α - and β -conformation of the 1'' oxygen atom of ADP-ribose coexist, the latter being more frequent (relative occupancy of 75%). These alter-

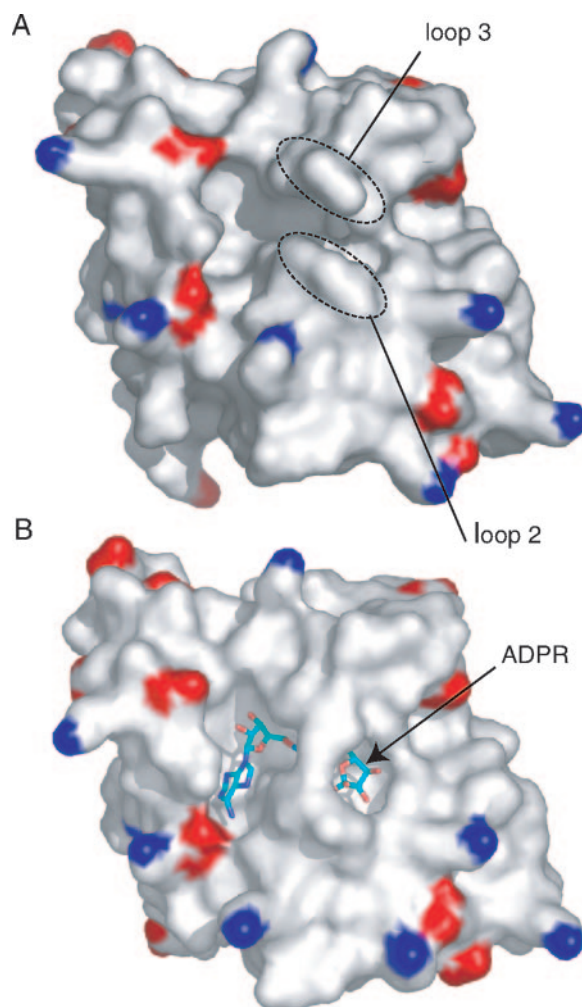


FIG. 3. Conformational changes upon ADP-ribose binding. Panels A and B display the surface of the SARS-CoV macro domain colored according to electrostatic potential (positive and negative charges are indicated in blue and red, respectively), in its unliganded (A) and ADP-ribose bound (B) forms. Upon ADP-ribose binding, conformational changes implicating mainly loops 2 and 3 result in a small closing of the pocket around its ligand.

native conformations are associated with alternative conformations of residues Gly-47 and Gly-48 of the glycine loop. The electron densities of both loops are well defined in the electron density for the three monomers, and the average temperature factor of the residues forming these loops is similar to that of the rest of the protein. However, the conformational changes observed in these loops upon ADP-ribose binding reveal their adaptability. Examination of the conformation of the equivalent loops in liganded and unliganded structures of *S. cerevisiae* and *A. fulgidus* macro domains also revealed that these loops have some flexibility.

Structural and mechanistic basis for ADP-ribose 1''-phosphatase activity. Both the SARS-CoV and HCoV-229E macro domain-associated ADP-ribose 1''-phosphatase activities have been discovered and characterized recently (30, 33). Moreover, in a recent study on the YMX7 yeast protein, a catalytic mechanism has been suggested, based on an Asp-His-Asn catalytic

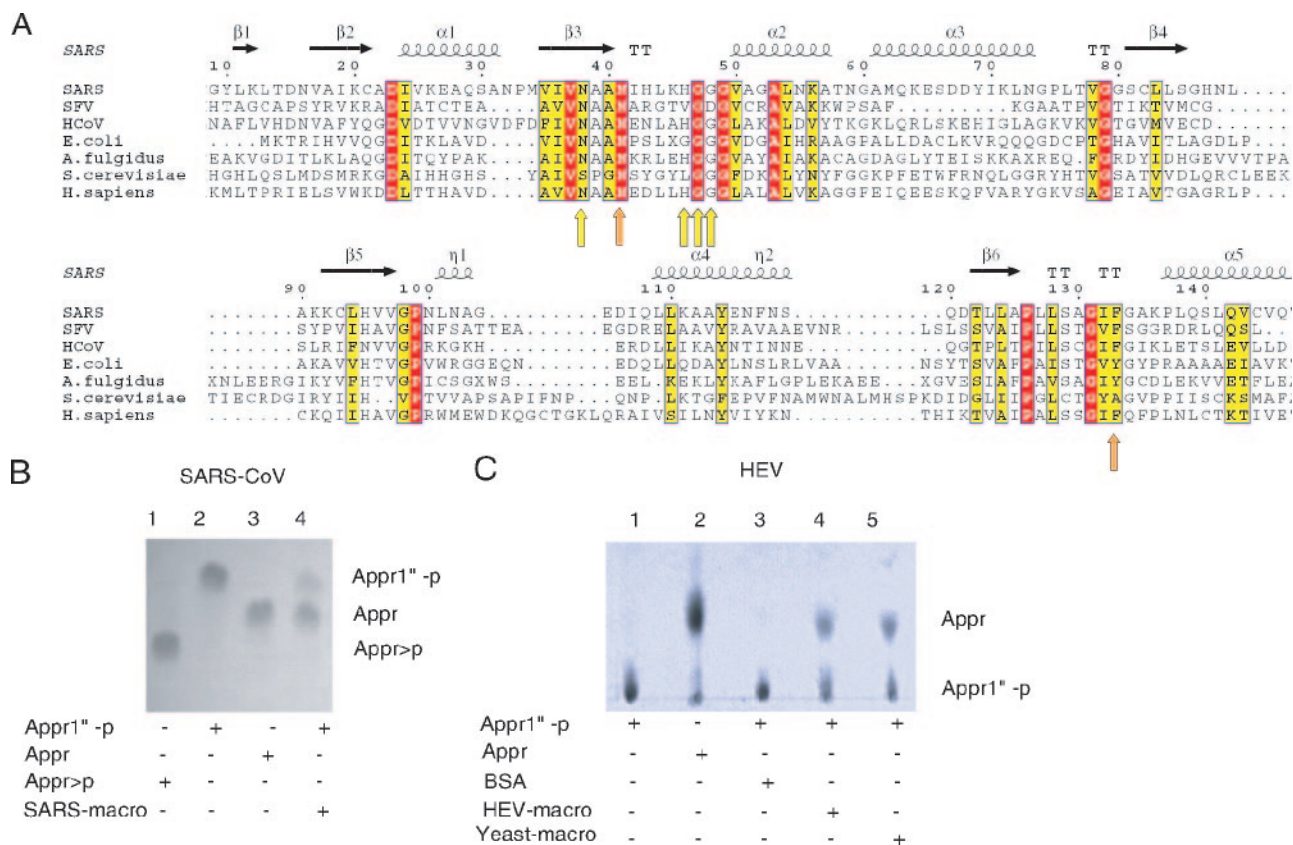


FIG. 4. ADP-ribose 1'-phosphatase activity of viral macro domains. (A) Structure-based sequence alignment of the SARS-CoV macro domain sequence with macro domain sequences from Semliki Forest virus nsP3 (SFV), HCoV-OC43 nsp3, *E. coli* (protein COG2110), *A. fulgidus* (protein AF1521), *Saccharomyces cerevisiae* (protein YMX7_YEAST), and human (protein mH2A1.1). Strictly conserved residues are boxed in red, whereas residues for which the consensus is >70% are boxed in yellow. Secondary structure elements of the SARS-CoV macro domain are represented above the alignment. Yellow and orange thick arrows below the alignment indicate amino acids whose mutation decrease (yellow) or abolish (orange) ADP-ribose phosphatase activity. These are referred to in the text and in Fig. 5A and B. (B) TLC assay on the SARS-CoV macro domain activity. Markers were loaded in lanes 1 to 3, and the reaction mixture (described in Materials and Methods) was loaded in lane 4. Abbreviations: ADP-ribose (Appr), ADP-ribose 1'-phosphate (Appr¹-p), ADP-ribose 1',2'-cyclic phosphate (Appr>p). (C) TLC assay on the HEV macro domain activity. Lanes 1 to 5 contain reaction mixtures as indicated below the chromatogram. Abbreviations are the same as in panel B. Bovine serum albumin (BSA) was used as a negative control, and the yeast macro domain protein Poa1p (lane 5) was used as a positive control.

triad (18). However, no experimental data has been used to test this hypothesis, and neither the Asp nor the His residues of the proposed catalytic triad are conserved among viral macro domains (e.g., Asp-90 is equivalent to SARS-CoV Ala-51 and His-145 is equivalent to an Asn residue in HCoV-229E [residue 95 in SARS-CoV numbering in Fig. 4A]). The nonconservation of key catalytic residues among these enzymes as well as the divergence of macro domain sequences inside the viral world prompted us to study the molecular determinants of ADP-ribose 1'-phosphatase activity. Both the SARS-CoV and the HEV macro domain were able to hydrolyze the ADP-ribose 1'-phosphate substrate (Fig. 4B and C). The enzymatic activity of the SFV macro domain was at the limit of detection (M. Heinonen and T. Ahola, unpublished data).

In order to get insight into the relevance of this activity, the ADP-ribose macro domain binary complex was used to identify residues in the vicinity of the C1' atom. An attempt was then made to model an ADP-ribose 1'-phosphate molecule into the putative active site in both conformations of the 1' oxygen atom revealed by the electron density map. Due to steric con-

straints, this resulted in a poor fit of the ADP-ribose 1'-phosphate (results not shown). This poor fit suggests that the macro domain exhibits a substrate affinity even lower than that observed for the hydrolysis product ADP-ribose or that the two structures presented here are in a conformation different from that required to bind the substrate of the phosphatase reaction. A number of residues likely to be involved in this reaction and/or in substrate binding were identified based on both their sequence conservation and C1' vicinity. These are Asn-38, Asn-41, His-46, Gly-47, Gly-48, Asn-102, and Phe-133. We then conducted a mutagenesis study to assess their relevance in promoting the phosphatase activity of the SARS-CoV macro domain (Fig. 5). Asn-41 substitution to alanine proved to abolish activity completely in our assay. It is also the only residue to fulfill the two criteria of both absolute conservation among macro domains of all kingdoms and vicinity of the C1' in the published structures. The other essential amino acid for the SARS-CoV macro domain activity is Phe-133. It is also conserved, except in alphaviruses, where it is replaced by a similar residue, a tyrosine. In contrast, Asp-23, for which a role in

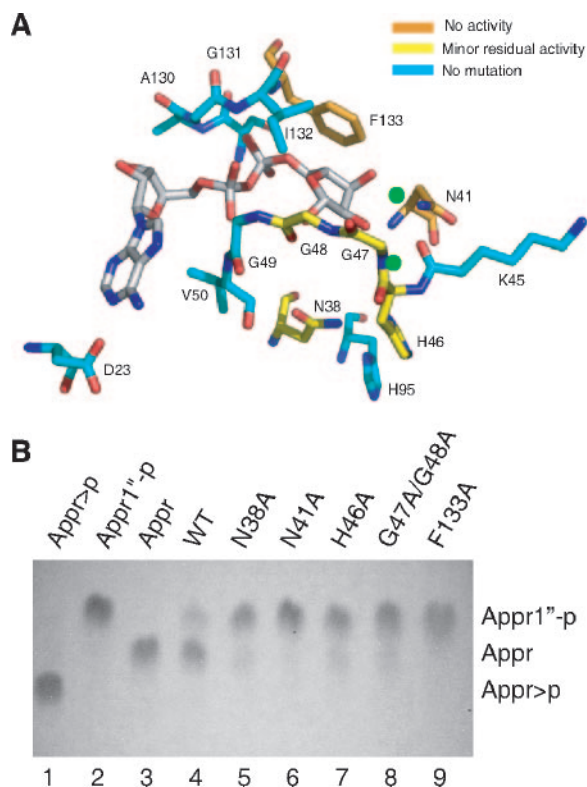


FIG. 5. Structural determinants for the SARS-CoV macro domain ADP-ribose 1'-phosphatase activity. (A) The ADP-ribose molecule and the amino acid residues from the binding pocket are represented in sticks. Carbon atoms from the ADP-ribose molecule are shown in white, whereas carbon atoms from the surrounding residues are colored according to their role in ADP-ribose 1'-phosphatase activity: orange when substitution of the residue to alanine abolished activity and yellow when minor activity persists upon replacement by an alanine. For residues that were not replaced, carbon atoms are displayed in cyan. The two water molecules present in the ADP-ribose binding pocket are shown as green spheres. (B) TLC assay. Abbreviations are the same as in Fig. 4. In the first three lanes, Appr>p, Appr1'-p, and Appr were loaded as markers. In lanes 4 to 9, wild-type enzyme and several mutants (N38A, N41A, H46A, G47A/G48A, and F133A) were tested for their ADP-ribose 1'-phosphatase activity as described in Materials and Methods.

adenosine specificity is apparent (Fig. 5A), is not conserved. Substitutions of the other previously mentioned residues had either no significant impact on activity (Asn-102) or only reduced (but did not abolish) activity under the experimental conditions used in this assay.

Mechanism for a promiscuous activity? Structural and mutagenesis experiments suggest that Asn-41 participates in catalysis, whereas Phe-133 might be involved in both binding the substrate and in catalysis, as suggested in other NAD binding proteins (23). The oxygen of the Asn-41 side chain tightly interacts via hydrogen bonds with three main chain NH groups and, as a result, the amino group of the side chain is precisely positioned within the active site pocket. It interacts with the 2' and 3' OH groups of the ribose moiety, with two main chain carbonyl oxygens and a water molecule that is conserved in all macro domain structures. This water molecule, in turn, interacts with the 2' and 3' OH groups of the ribose moiety and is

maintained in its position via three hydrogen bonds with main chain atoms. This water molecule could indeed promote a nucleophilic attack on the phosphorus of the ADP-ribose 1'-monophosphate. Other residues are only partially conserved among macro domains. Thus, a single residue (Asn-41) is the signature of an active ADP-ribose 1'-phosphatase.

Nevertheless, there are a number of puzzling questions concerning the authentic function of viral macro domains (see Discussion). The recent demonstration of ADP-ribose and PAR-binding functions of an archaeal macro domain (17) prompted us to investigate the latter function.

Poly(ADP-ribose) binding. Poly(ADP-ribosyl)ation is a post-translational modification of proteins. This modification, which governs several fundamental processes of cell life, involves a covalent binding of poly(ADP-ribose) (PAR) to a target protein. When triggered by a viral infection (reviewed in reference 15), poly(ADP-ribosyl)ation acts as a stress signal in order to induce apoptosis and/or necrosis in the cell. We tested the ability of viral macro domains to bind PAR using PARP-1-synthesized PAR (Fig. 6). The SARS-CoV macro domain was able to bind radiolabeled PAR in solution, and the amount of coprecipitated PAR on beads was proportional to the amount of SARS-CoV macro domain (Fig. 6A). PARP-1-linked PAR binding was also assayed by using a filter binding assay (Fig. 6B).

All three viral macro domains were found to bind PAR, the SFV macro domain being the strongest PAR binder. The involvement of the PARP-1 protein as the macro domain binder was ruled out when purified PAR was used in the filter-binding assay. All three macro domains were able to bind PARP-1-free PAR (Fig. 6C). We conclude that viral macro domains are PAR-binding modules and that this activity does not necessarily correlate with their ADP-ribose 1'-phosphatase activities.

Model of poly(ADP-ribose) binding. How could the PAR be accommodated onto the macro domain? A model of di-ADP-ribose was constructed, and its possible mode of binding was examined by using molecular modeling (Fig. 7). A second ADP-ribose was added to the ribose 2' position of the experimentally positioned ADP-ribose, linked by an α -1" bond. The position of the original ADP-ribose was maintained in order to rely on experimental data. Two potential binding modes could be inferred for the second ADP-ribose. In both cases, the proximal ribose of the second ADP-ribose moiety is positioned in a groove immediately adjacent to the ADP-ribose-binding crevice. This proximal ribose is surrounded by five residues (Leu-127, Gly-131, Asn-157, Asp-158, and Leu-161), with one of them (Gly-131) being conserved among all macro domains. Leu-127 is well conserved in RNA virus macro domains only. The phosphate groups are not positioned in the groove but are located near the main chain amino groups of Ile-132 and Gly-49. The distal ribose and the adenosine of the second ADP-ribose moiety can be positioned according to two possibilities. In the first model, they are located near Gly-47, Gly-48, Val-50, Ala-51, Gly-52, Ala-56, and Lys-56. Among these residues, Gly-47 and Ala-53 are conserved in RNA virus macro domains, as well as in *E. coli*, *A. fulgidus*, and yeast. Ala-50 is well conserved in RNA virus macro domains, in *A. fulgidus*, and in macroH2A1.1. In the second model, residues located in the vicinity of the adenosine (Ala-30, Gly-134, Ala-135, and Lys-136) are part of a more variable region of macro domains, thus

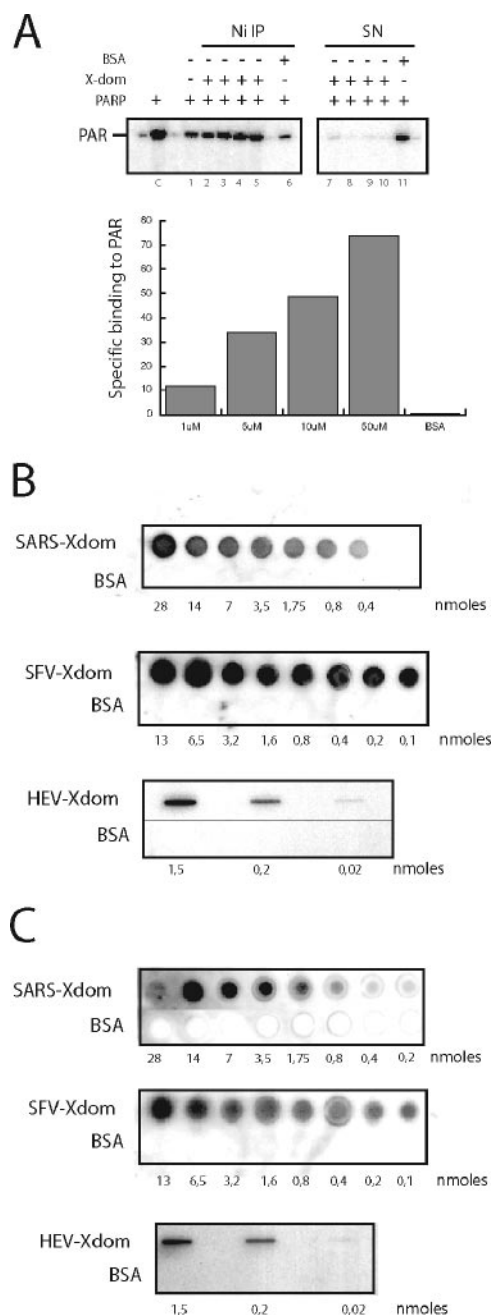


FIG. 6. SARS-CoV, SFV, and HEV macro domains bind poly-(ADP-Ribose) in vitro. (A) Ni precipitation of PAR bound to His-tagged SARS-CoV macro domain. BSA (50 μ M, lanes 6 and 11) or increasing concentrations of the SARS-CoV macro domain (1 μ M, lanes 2, 8, and 7; 5 μ M, lanes 3, 9, and 8; 10 μ M lanes 4, 10, and 9; 50 μ M, lanes 5, 11, and 10) were incubated with radiolabeled PAR synthesized using hPARP-1 (lanes 2 to 11) and subsequently precipitated with Ni-beads (lanes 2 to 6). Unbound complexes present in the supernatant after Ni precipitation are shown in lanes 7 to 11. The amount of the radiolabeled PAR synthesized using hPARP-1 is shown as a control (lane c), and the amount of unspecific binding of PAR to Ni-beads is shown in lane 1. Migration position of PAR is shown on the left. After quantification, the ratio of the amount of PAR present after Ni precipitation over that present in the supernatant was calculated and used to determine the specific binding of PAR to the SARS-CoV macro domain. (B) 32 P-labeled PAR-labeled PARP-1 was incubated with nitrocellulose membranes containing increasing concentrations of dot-blotted SARS-CoV, SFV, or HEV macro domains or BSA, which

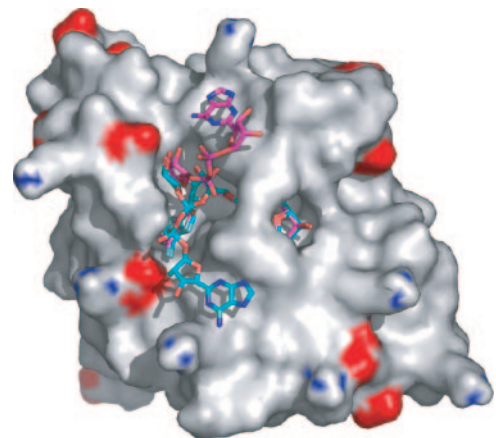


FIG. 7. Model for PAR binding. Based on the position of ADP-ribose as observed in the crystal structure, modeling studies were performed to accommodate a di-ADP-ribose. One conformation for each of the best two clusters is represented in sticks (carbon atoms in pink and cyan, respectively). The SARS-CoV macro domain surface is colored as in Fig. 3.

arguing in favor of the first binding-mode model. The modeling of di-ADP ribose on the *A. fulgidus* crystal structure, which also binds poly(ADP ribose), leads to the same two clusters and thus to the same conclusions (data not shown).

DISCUSSION

Macro domains are found in organisms from all kingdoms of life, and it is thus assumed that they play fundamental and perhaps universal roles in the perpetuation or expression of genetic information. Although the sequence signatures of these domains were detected a while ago, their function remained elusive until a genome-wide screen of yeast proteins showed that the yeast macro domain protein Poa1p could carry out a specialized ADP-ribose phosphoesterase activity (22). Poa1p is not closely related to any known phosphatase, and it is quite specific for ADP-ribose 1''-phosphate, a by-product of tRNA splicing pathway, with a turnover constant of 1.7 min⁻¹ (37). Such a value is rather low for an enzyme putatively involved in regulating the concentration of a metabolite, as the enzyme might be unable to cope efficiently with abrupt metabolite concentration variations. Subsequently, the crystal structure of an archaeal macro domain revealed that it shares structural features with P-loop-containing nucleotide triphosphate hydrolases (2).

Specific ADP-ribose 1''-phosphatase activity has been recently described for three positive-strand RNA viruses of the *Coronaviridae* genus (31), also with a modest turnover constant of 5 to 20 min⁻¹. Our present study confirms that viral macro domains are indeed able to hydrolyze ADP-ribose 1''-phos-

was used as a negative control. For each membrane, the same amount, indicated under the blot, of viral macro domain or control BSA was blotted. The membranes were analyzed by phosphorimaging. (C) Same experiment as in panel B except that membranes were incubated with 32 P-labeled PAR purified after DNase and proteinase K treatment.

phate. However, in our opinion, the available evidence does not sufficiently support a scenario in which this phosphatase activity would represent the sole biologically relevant function of the macro domain *in vivo*. In line with this idea, the enzymatic activity of the coronavirus macro domain is dispensable for viral RNA synthesis and virus reproduction under cell culture conditions (30). There are several lines of evidence that suggest functions other than ADP-ribose 1"-phosphatase for viral macro domains. First, viral (and cellular) macro domains are not closely related to other known phosphatases. The method of the discovery of the activity might well have been misleading. The phosphatase activity was discovered by a genome-wide search for this particular activity and not by a phenotype-guided search. Deletion of the *POA1* gene in yeast had no detectable phenotype under various growth conditions, suggesting a role in a temporary or minor pathway (37). The macro domain-containing viruses replicate in the cytoplasm of the infected cell and do not appear to use nuclear tRNA splicing pathways that generate ADP-ribose 1"-phosphate, the putative substrate of macro domains. To our knowledge, there is nothing to suggest that such a substrate would be generated during RNA virus replication.

Second, even key amino acids close to the putative catalytic center are not conserved, suggesting different specific activities for the large variety of viral and cellular macro domains. We are left with questions, such as why should a conserved catalytic activity thought to be involved in metabolic regulation be based on nonconserved catalytic residues? Why do the catalytic efficiencies observed for these structurally and evolutionary conserved macro domains differ so widely?

Third, in animal cells, macro domains are often found associated physically with PARP, an enzyme involved in poly(ADP-ribose) metabolism. The recent demonstration that the archaeal macro domain AF1521 is an ADP-ribose and poly(ADP-ribose) binding module is in full agreement with our corresponding proposition for such a function for viral macro domains (17). In the case of AF1521, ADP-ribose is the best inhibitor (50% inhibitory concentration of $\sim 30 \mu\text{M}$) of the ADP-ribose 1"-phosphatase activity and the K_D for ADP-ribose is around 126 nM, i.e., ~ 200 -fold lower than that of the SARS-CoV macro domain studied here ($K_D \sim 24 \mu\text{M}$). The discovery of poly(ADP-ribose) binding (17) is important in that it casts a new light on the possible role of macro domains also in the viral world. Our work shows that the ADP-ribose binding site adopts two conformations, in which the ADP-ribose (putative product) clearly fits much better than ADP-ribose 1"-phosphate (putative substrate). Altogether, we favor the hypothesis that the hydrolysis of ADP-ribose 1"-phosphate might well be one result of evolution, whereas poly(ADP-ribose) binding might be another.

These considerations prompted us to assay poly(ADP-ribose) binding by several viral macro domains. Indeed, they were subsequently found to be robust poly(ADP-ribose) binding modules and, interestingly, the poorly active SFV ADP-ribose 1"-phosphatase turned out to be the most efficient free and PARP-1-linked poly(ADP-ribose) binding module relative to its fellow coronavirus and HEV counterparts (Fig. 6). The structural model of bound di-ADP-ribose indicates that such a unit could bind to a groove present on the surface of the macro domain, lined with conserved amino acid residues in coronaviruses (Fig. 7).

There are a number of questions concerning the role of these macro domains during the course of a viral infection. In alphaviruses, involvement in the cell response to infection has also been proposed (8). The macro domain-containing viruses have a cytoplasmic replication cycle, and their macro domain proteins do not appear to enter into the nucleus (reviewed in reference 34), raising the question of whether or not the nuclear PARP-1 activity is relevant for their functions. The alphavirus Sindbis virus was one of the first viruses shown to induce cell apoptosis during fusion and entry. Membrane depolarization induces a cascade of events involving many partners such as nuclear factor κB and various phospholipases leading to NAD^+ and ATP depletion, activation of the nuclear PARP-1, and eventual cell death (reference 26 and references therein). Thus, the infected cell sends signals to the nucleus to regulate protein function by poly(ADP-ribosyl)ation in response to the infection. Even though PARP-1 is a nuclear enzyme, cross talk with the mitochondria has been demonstrated (reference 36 and references therein). Thus, the presence of the macro domain in cytoplasmic viral proteins raises the question about the existence of a cytoplasmic poly(ADP-ribosyl)ated messenger. One possibility is that this poly(ADP-ribosyl)ated messenger would be exported from the nucleus and intercepted by the viral macro domain, perhaps to stop ATP depletion and maintain the nucleotide pools required for active viral RNA synthesis (26). There are 17 members of the PARP family in the human genome, and the majority remains completely uncharacterized with respect to function and localization (28). Of the characterized PARPs, at least vault PARPs (VPA, also known as PARP-4) and tankyrases are partially localized in the cytoplasm (27). Interestingly, one of the PARP family members was originally identified as the zinc finger antiviral protein (11). It is also active against alphaviruses (3), but its putative PARP activity remains uncharacterized. It is an intriguing possibility that one or several of the novel PARPs might be located in the cytoplasm and be the target of viral macro domains, suggesting that the poly(ADP-ribose) binding function identified here may lead to the discovery of novel cell-virus interaction pathways.

ACKNOWLEDGMENTS

This study was supported, in part, by the Genopole Marseille-Nice, the SPINE project of the European Union 6th PCRDT (QLRT-2001-00988), and subsequently by the Euro-Asian SARS-DTV Network (SP22-CT-2004-511064) and the European Commission specific research and technological development Programme "Integrating and Strengthening the European Research Area" and the VIZIER integrated project (LSHG-CT-2004-511960) from the European Union 6th PCRDT. M.H. and T.A. acknowledge the financial support of the Academy of Finland (grant 201687), Sigrid Juselius Foundation, and Helsinki University Research Funds.

REFERENCES

1. Aguiar, R. C., K. Takeyama, C. He, K. Kreinbrink, and M. A. Shipp. 2005. B-aggressive lymphoma family proteins have unique domains that modulate transcription and exhibit poly(ADP-ribose) polymerase activity. *J. Biol. Chem.* **280**:33756–33765.
2. Allen, M. D., A. M. Buckle, S. C. Cordell, J. Lowe, and M. Bycroft. 2003. The crystal structure of AF1521 a protein from *Archaeoglobus fulgidus* with homology to the non-histone domain of macroH2A. *J. Mol. Biol.* **330**:503–511.
3. Bick, M. J., J. W. Carroll, G. Gao, S. P. Goff, C. M. Rice, and M. R. MacDonald. 2003. Expression of the zinc-finger antiviral protein inhibits alphavirus replication. *J. Virol.* **77**:11555–11562.
4. Brierley, I., P. Digard, and S. C. Inglis. 1989. Characterization of an efficient

- coronavirus ribosomal frameshifting signal: requirement for an RNA pseudoknot. *Cell* **57**:537–547.
5. Cohen, S. X., R. J. Morris, F. J. Fernandez, M. Ben Jelloul, M. Kakaris, V. Parthasarathy, V. S. Lamzin, G. J. Kleywegt, and A. Perrakis. 2004. Towards complete validated models in the next generation of ARP/wARP. *Acta Crystallogr. D Biol. Crystallogr.* **60**:2222–2229.
 6. Collaborative Computational Project. 1994. T programs for protein crystallography. *Acta Crystallogr. D Biol. Crystallogr.* **50**:760–763.
 7. Cuff, J. A., M. E. Clamp, A. S. Siddiqui, M. Finlay, and G. J. Barton. 1998. JPred: a consensus secondary structure prediction server. *Bioinformatics* **14**:892–893.
 8. De, L., C. Fata-Hartley, S. G. Sawicki, and D. L. Sawicki. 2003. Functional analysis of nsP3 phosphoprotein mutants of Sindbis virus. *J. Virol.* **77**:13106–13116.
 9. Edgar, R. C. 2004. MUSCLE: multiple sequence alignment with high accuracy and high throughput. *Nucleic Acids Res.* **32**:1792–1797.
 10. Galtier, N., M. Gouy, and C. Gautier. 1996. SEAVIEW and PHYLO_WIN: two graphic tools for sequence alignment and molecular phylogeny. *Comput. Appl. Biosci.* **12**:543–548.
 11. Gao, G., X. Guo, and S. P. Goff. 2002. Inhibition of retroviral RNA production by ZAP, a CCCH-type zinc finger protein. *Science* **297**:1703–1706.
 12. Gorbalenya, A. E., L. Enjuanes, J. Ziebuhr, and E. J. Snijder. 2006. Nidovirales: evolving the largest RNA virus genome. *Virus Res.*, in press.
 13. Gorbalenya, A. E., E. V. Koonin, and M. M. Lai. 1991. Putative papain-related thiol proteases of positive-strand RNA viruses. Identification of rubi- and aphthovirus proteases and delineation of a novel conserved domain associated with proteases of rubi-, alpha-, and coronaviruses. *FEBS Lett.* **288**:201–205.
 14. Gouet, P., E. Courcelle, D. I. Stuart, and F. Metz. 1999. ESPript: analysis of multiple sequence alignments in PostScript. *Bioinformatics* **15**:305–308.
 15. Hay, S., and G. Kannourakis. 2002. A time to kill: viral manipulation of the cell death program. *J. Gen. Virol.* **83**:1547–1564.
 16. Holm, L., and C. Sander. 1995. Dali: a network tool for protein structure comparison. *Trends Biochem. Sci.* **20**:478–480.
 17. Karras, G. I., G. Kustatscher, H. R. Buhecha, M. D. Allen, C. Pugieux, F. Sait, M. Bycroft, and A. G. Ladurner. 2005. The macro domain is an ADP-ribose binding module. *EMBO J.* **24**:1911–1920.
 18. Kumaran, D., S. Eswaramoorthy, F. W. Studier, and S. Swaminathan. 2005. Structure and mechanism of ADP-ribose-1"-monophosphatase (Appr-1"-pase), a ubiquitous cellular processing enzyme. *Protein Sci.* **14**:719–726.
 19. Kustatscher, G., M. Hothorn, C. Pugieux, K. Scheffzek, and A. G. Ladurner. 2005. Splicing regulates NAD metabolite binding to histone macroH2A. *Nat. Struct. Mol. Biol.* **12**:624–625.
 20. Laskowski, R. A., M. W. MacArthur, D. S. Moss, and J. M. Thornton. 1993. PROCHECK: a program to check the stereochemical quality of protein structures. *J. Appl. Crystallogr.* **26**:283–291.
 21. Malet, H., K. Dalle, N. Bremond, F. Tocque, S. Blangy, V. Campanacci, B. Coutard, S. Grisel, J. Lichiere, V. Lantze, C. Cambillau, B. Canard, and M. Egloff. 2006. Expression, purification and crystallization of the SARS-CoV macro domain. *Acta Crystallogr. Sect. F* **62**:405–408.
 22. Martzen, M. R., S. M. McCraith, S. L. Spinelli, F. M. Torres, S. Fields, E. J. Grayhack, and E. M. Phizicky. 1999. A biochemical genomics approach for identifying genes by the activity of their products. *Science* **286**:1153–1155.
 23. Min, J., J. Landry, R. Sternglanz, and R. M. Xu. 2001. Crystal structure of a SIR2 homolog-NAD complex. *Cell* **105**:269–279.
 24. Morris, G. M., D. S. Goodsell, R. S. Halliday, R. Huey, W. E. Hart, R. K. Belew, and A. J. Olson. 1998. Automated docking using a Lamarckian genetic algorithm and empirical binding free energy function. *J. Comput. Chem.* **19**:1639–1662.
 25. Murshudov, G. N., A. A. Vagin, and E. J. Dodson. 1997. Refinement of macromolecular structures by the maximum-likelihood method. *Acta Crystallogr. D Biol. Crystallogr.* **53**:240–255.
 26. Nargi-Aizenman, J. L., C. M. Simbulan-Rosenthal, T. A. Kelly, M. E. Smulson, and D. E. Griffin. 2002. Rapid activation of poly(ADP-ribose) polymerase contributes to Sindbis virus and staurosporine-induced apoptotic cell death. *Virology* **293**:164–171.
 27. Nguewa, P. A., M. A. Fuertes, B. Valladares, C. Alonso, and J. M. Perez. 2005. Poly(ADP-ribose) polymerases: homology, structural domains, and functions: novel therapeutic applications. *Prog. Biophys. Mol. Biol.* **88**:143–172.
 28. Otto, H., P. A. Reche, F. Bazan, K. Dittmar, F. Haag, and F. Koch-Nolte. 2005. In silico characterization of the family of PARP-like poly(ADP-ribose) transferases (pARTs). *BMC Genomics* **6**:139.
 29. Pehrson, J. R., and V. A. Fried. 1992. MacroH2A, a core histone containing a large nonhistone region. *Science* **257**:1398–1400.
 30. Putics, A., W. Filipowicz, J. Hall, A. E. Gorbalenya, and J. Ziebuhr. 2005. ADP-ribose-1"-monophosphatase: a conserved coronavirus enzyme that is dispensable for viral replication in tissue culture. *J. Virol.* **79**:12721–12731.
 31. Putics, A., A. E. Gorbalenya, and J. Ziebuhr. 2006. Identification of protease and ADP-ribose 1"-monophosphatase activities associated with transmissible gastroenteritis virus nonstructural protein 3. *J. Gen. Virol.* **87**:651–656.
 32. Roussel, A., and C. Cambillau. 1991. Silicon graphics directory, p. 97. Silicon Graphics, Mountain View, Calif.
 33. Saikatendu, K. S., J. S. Joseph, V. Subramanian, T. Clayton, M. Griffith, K. Moy, J. Velasquez, B. W. Neuman, M. J. Buchmeier, R. C. Stevens, and P. Kuhn. 2005. Structural basis of severe acute respiratory syndrome coronavirus ADP-ribose-1"-phosphate dephosphorylation by a conserved domain of nsP3. *Structure* **13**:1665–1675.
 34. Salonen, A., T. Ahola, and L. Kaariainen. 2005. Viral RNA replication in association with cellular membranes. *Curr. Top. Microbiol. Immunol.* **285**:139–173.
 35. Schuttelkopf, A. W., and D. M. van Aalten. 2004. PRODRG: a tool for high-throughput crystallography of protein-ligand complexes. *Acta Crystallogr. D Biol. Crystallogr.* **60**:1355–1363.
 36. Scovassi, A. I. 2004. Mitochondrial poly(ADP-ribosylation): from old data to new perspectives. *FASEB J.* **18**:1487–1488.
 37. Shull, N. P., S. L. Spinelli, and E. M. Phizicky. 2005. A highly specific phosphatase that acts on ADP-ribose 1"-phosphate, a metabolite of tRNA splicing in *Saccharomyces cerevisiae*. *Nucleic Acids Res.* **33**:650–660.
 38. Siddell, S. G., J. Ziebuhr, and E. J. Snijder. 2005. Coronaviruses, toroviruses, and arteriviruses, p. 823–856. In B. W. J. Mahy and V. ter Meulen (ed.), Topley and Wilson's microbiology and microbial infections, 10th ed., vol. 1. Hodder Arnold, London, United Kingdom.
 39. Snijder, E. J., P. J. Bredenbeek, J. C. Dobbe, V. Thiel, J. Ziebuhr, L. L. Poon, Y. Guan, M. Rozanov, W. J. Spaan, and A. E. Gorbalenya. 2003. Unique and conserved features of genome and proteome of SARS-coronavirus, an early split-off from the coronavirus group 2 lineage. *J. Mol. Biol.* **331**:991–1004.
 40. Terwilliger, T. C. 2002. Automated structure solution, density modification and model building. *Acta Crystallogr. D Biol. Crystallogr.* **58**:1937–1940.
 41. Terwilliger, T. C., and J. Berendzen. 1999. Automated MAD and MIR structure solution. *Acta Crystallogr. D Biol. Crystallogr.* **55**(Pt. 4):849–861.
 42. Thiel, V., K. A. Ivanov, A. Putics, T. Hertzog, B. Schelle, S. Bayer, B. Weissbrich, E. J. Snijder, H. Rabenau, H. W. Doerr, A. E. Gorbalenya, and J. Ziebuhr. 2003. Mechanisms and enzymes involved in SARS coronavirus genome expression. *J. Gen. Virol.* **84**:2305–2315.
 43. Ziebuhr, J., V. Thiel, and A. E. Gorbalenya. 2001. The autocatalytic release of a putative RNA virus transcription factor from its polyprotein precursor involves two paralogous papain-like proteases that cleave the same peptide bond. *J. Biol. Chem.* **276**:33220–33232.